To be published in IEEE
Trans. on Nuclear Science

LBL-399
Preprint

PERFORMANCE STUDIES OF PHOTOMULTIPLIERS HAVING DYNODES WITH GaP(Cs) SECONDARY EMITTING SURFACE

B. Leskovar and C. C. Lo

February 1972

AEC Contract No. W-7405-eng-48

DISCLAIMER

PERFORMANCE STUDIES OF PHOTOMULTIPLIERS HAVING DYNODES WITH GaP(Cs) SECONDARY EMITTING SURFACE

B. Leskovar, C. C. Lo
Lawrence Berkeley Laboratory, University of California
Berkeley, California

Summary

Characteristics of photomultipliers having dynodes with cesium-activated gallium phosphide secondary emitting surfaces have been investigated. We present measurements of characteristics, generally not available from manufacturers' data sheets, for several 8850's, C70133B's, 8852's, and C31024's. The transit-time difference, the single-electron transit-time spread, and the collection and quantum efficiency uniformity as a function of the position of the photocathode sensing area are measured and discussed. Measurement techniques and descriptions of measuring systems are given in detail. Emphasis is put on the determination of optimum photomultiplier operating conditions, particularly concerning the collection efficiency, and minimum transit-time spread.

Introduction

Secondary emission limitations which result from the short escape depth of electrons in conventional secondary emitters are reduced considerably by use of cesium activated gallium-phosphide secondary emitters. It was shown by R. E. Simon and B. F. Williams[1] that in GaP(Cs) emitters a reduction of the surface barrier and the bending of energy bands occur when the electropositive cesium is deposited on the heavily doped p-type crystal of gallium phosphide. Under these conditions, electron affinity is smaller than the band gap of GaP. Furthermore, electrons can pass through the bent-band region with a small loss in energy. Therefore, such a configuration behaves as if it has a negative electron affinity and consequently a high secondary emission yield. In addition, the secondary emission gain increases linearly with increasing primary energy up to very high voltages.

This paper presents and discusses performance characteristics measurements of photomultipliers having dynodes with cesium-activated gallium-phosphide secondary emitting surfaces. Secondary-emission yields of the GaP(Cs) surface are considerably higher, typically between 30 and 50 at a primary electron energy of 600 eV, than those obtained with conventional dynode materials, where average dynode gains of 5 to 8 can be achieved.[2,3] Because the electron resolution of a photomultiplier depends primarily upon the average gain of the first dynode and the distribution in number of secondary electrons, a higher electron resolution has been achieved, together with better dark-pulse distribution, decreased anode pulse rise time due to the fewer number of stages, and increased time resolution capabilities. Consequently, photomultipliers having dynodes with a GaP(Cs) secondary emitting surface are suitable for low-energy scintillation counting and for generating signals required in certain experimental research areas, where the device used for generating signals should absorb a minimum energy from the particles being studied, having at the same time very small spurious signal response.

Based on previous work,[4,5,6] further effort has been expanded to include measurement of characteristics, generally not available from manufacturers' data sheets, and to determine optimum operating conditions concerning the collection efficiency and electron transit time spread, for several 8850's, C70133B's, 8852's, and C31024's. Photomultipliers 8850, C70133B and 8852 have the first dynode with GaP(Cs) secondary emitting surface, followed by conventional copper-beryllium dynodes in the succeeding stages. The photomultiplier C31024 has all dynodes with a GaP(Cs) emitting surface. Measurements were made using the voltage divider network suggested by RCA for a particular photomultiplier. The operating voltage was 2500 V for 8850, 8852, and C70133B photomultipliers and 3500 V for C31024's. All photomultipliers were demagnetized and shielded before measurements. Furthermore, typical photomultiplier characteristics, such as gain, dark current, anode output current, transit and rise time as a function of voltage between anode and cathode, and photoelectron pulse height spectrum were measured and compared with the data provided by the manufacturer. For all photomultipliers, typical measured characteristics were inside production tolerances specified by the manufacturer.

Electron Transit Time Difference

Electron transit time difference is the difference in transit time between electrons leaving the center of photocathode and electrons leaving the photocathode at some specified point. In a typical photocathode design, the transit time is longer for edge illumination than for center illumination because edge trajectories are longer than axial trajectories, due to the weaker electrical field at the edge. Generally, transit-time difference information, although important, is not available from photomultiplier manufacturers.

A block diagram of the system for measuring electron transit-time difference is given in Fig. 1A. A light-emitting diode (LED, Ferranti type PD5002), driven by an avalanche transistor pulse generator, was used as the light source. A positioning disc with 3.2 mm holes spaced 4 mm apart, along lines parallel to and perpendicular to the long axis of the first dynode, was attached to the photomultiplier window. To prevent the electromagnetic field of the light pulser from interfering with photomultiplier operation, a 12-inch long American Optical LG3 light guide was used to guide the light pulse to the photocathode. Whenever a particular area of the photocathode was chosen to be illuminated, the light guide was placed in a corresponding hole of the positioning disc. The successive scanning was done along X and Y axes, with the longer side of the rectangular first dynode as the X axis. The exact position designations of the first dynode are given in Figs. 2-13. The illuminated area of the photocathode was no larger than 1.6 mm in diameter. A 50-ohm clipping stub connected at the photomultiplier anode differentiated the output pulse, producing a zero-crossing signal. For measurements of photomultiplier C31024 electron transit time difference, an auxiliary anode bias supply, a variable attenuator, and two wideband amplifiers were inserted at points a and b. The auxiliary anode bias supply was needed

for obtaining peak linear anode pulse currents of approximately 75 mA from the C31024. The dependence of the peak anode current upon the anode bias voltage is given in Fig. 1B. In this particular case the clipping stub was connected at the output of the wideband amplifier. Zero-crossing pulses were processed in a modified Lawrence Berkeley Laboratory zero-crossing discriminator. The discriminator had a time walk of ± 50 psec over a 60 mv to 2 V input pulse amplitude variation in the worst case. The discriminator output was applied to a time-to-height converter via a discriminator-pulse shaper. The reference time pulse was obtained from the light pulser and was passed through a delay line and a discriminator. The discriminator was followed by the time-to-height converter whose output pulses were applied to a 400-channel pulse-height analyzer. The channel with the maximum number of counts was used to determine the value of the photomultiplier electron transit-time difference. Approximately 5 x 10^5 pulses were taken at each illuminated spot of the photocathode.

The timing error of the system shown in Fig. 1, which was contributed by the associated electronics, was approximately 30 psec FWHM. This error was reduced by almost a factor of two by averaging data from four successive measurements for each type of photomultiplier evaluated.

The measured electron transit time difference as a function of the position of the photocathode sensing area along the X and Y axes for 8850, 8852, C70133B and C31024 is shown in Figs. 2-5, respectively. However, it is interesting to note that the shapes of the electron transit time difference curves, obtained from several tubes of the same type, are basically similar. Curves differ in details and in their maximum and minimum values. The electron transit time difference is ultimately limited by the initial-velocity distribution of emitted electrons from the photocathode.

Single Electron Time Spread Measurements

The measurement of the single electron time spread was done by the system shown in Fig. 1. The system is described in the electron transit time difference measurement section. Actually, the electron transit time difference and the single electron time spread measurements were done at the same time. The channel with the maximum number of counts was used to determine the amount of electron transit time difference, while the single electron time spread of each of the spectra was calculated from the printout data, using the full width at half maximum amplitude (FWHM) points. The time spread was measured as a function of the position of the photocathode sensing area and for the full-photocathode illumination.

The light level of the light pulse generator was adjusted to a low intensity to generate predominantly single-photoelectron events. The electrical pulse driving the light pulse generator had a FWHM of approximately 400 psec and rise time of 350 psec. It was estimated that the FWHM of the light pulse was approximately 250 psec due to the fact that the light emitting diode was operated in the reverse-biased mode. Because of the very low counting efficiency in this case, typically 1%, the repetition frequency of light pulses was 100 kHz. Single electron time spread as a function of the position of the photocathode sensing area along the X and Y axes for 8850, 8852, C70133B, and C31024 is shown in Figs. 6-9, respectively. It can be seen from Fig. 8 that the electron time spread variation is less than $^{+0.95}_{-1.3}$ nsec within 55 mm of the center of the photocathode for C70133B. Furthermore, it can be seen from Figs. 6-9, that the electron time spread variation is less than $^{+0.2}_{-0.4}$ nsec, $^{+0.25}_{-0.5}$ nsec, and $^{+0.24}_{-0.15}$ nsec, within 18 mm of the center of the photocathode for photomultipliers 8850, 8852, and C31024, respectively. With full photocathode illumination the single electron time spread FWHM was 0.64 nsec, 0.81 nsec, 2.42 nsec, 0.57 nsec for photomultipliers 8850, 8852, C70133B, and C31024, respectively. The single electron time spread spectrum under full photocathode illumination condition for 8850, 8852, C70133B, and C31024 photomultipliers is given in Figs. 10-13, respectively.

Relative Anode Pulse Amplitude Measurements

Relative anode pulse amplitude measurements give information on the response uniformity of the product of quantum efficiency and collection efficiency at various illuminated areas on the photocathode. A block diagram of the system for measuring the relative anode pulse amplitude is given in Fig. 18. A positioning disc with 3.2 mm holes spaced 4 mm apart, in a direction parallel to the long direction of the first dynode through the center of the photocathode, and in a direction perpendicular to the first dynode, was attached to the photomultiplier window. A light emitting diode, PD5002, driven by an avalanche transistor pulse generator, was used as a light source. To reduce output pulse amplitude jitter a relatively higher level of emitting light was used. However, the peak value of the anode pulse current was kept inside the linear range of the photomultiplier output current. The amplitude of the light pulses was kept constant during the measurement. A fiber optics light guide, LG3, was used to guide the light pulse to a particular area on the photocathode. The signal from the light pulse generator was applied through a delay line to a discriminator, whose output was in coincidence with the photomultiplier output pulse. Both signals, from photomultiplier anode and light pulse generator, were applied to a linear gate to reduce the photomultiplier noise-pulse rate. A successive scanning of the photocathode was done, and photomultiplier output pulses were applied to the multichannel analyzer through a linear gate. The channel with the maximum number of counts, which was taken at the photocathode center, was used as a reference amplitude. The reference amplitude was compared with anode pulse amplitudes determined for different illuminated areas on the photocathode.

The results of these measurements are given in Figs. 14-17, for 8850, 8852, C70133B, and C31024, respectively. The solid lines show the relative anode pulse amplitude obtained when the photomultiplier was scanned with a light spot in a direction parallel to the long direction of the first dynode and through the center of the photocathode. The dashed curves are a result of scanning in a direction perpendicular to the first dynode. It is seen from Figs. 14, 15, and 17 that the relative anode pulse amplitudes vary within $^{+20\%}_{-5\ \%}$ for a distance ± 18 mm measured from the center of the photocathode of 8850, 8852 and C31024 photomultipliers. It is shown in Fig. 16 that the anode pulse

amplitudes varied within $^{+90\%}_{-40\%}$ for a distance ± 55 mm for photomultiplier C70133B. The largest anode pulse variations occurred at the edge of the photocathode, due primarily to reduced collection efficiency. For C31024 anode pulse amplitude measurements, the auxiliary bias supply, variable attenuator, and wideband amplifiers were inserted at points a and b to obtain linearity at high peak values of anode pulse current.

Relative Collection Efficiency Measurements and Optimization of Single Electron Time Spread

The relative collection efficiency measurements and an optimization of single electron time spread was done by the system shown in Fig. 18. The system was described in the previous section. Relative collection efficiency is defined as the ratio between the efficiency of counting light pulses at any input electron optics lens potential and the efficiency of counting light pulses at optimum potential of the input electron optics lens.

The collection efficiency varies with the potential distribution in the input electron optics and its value can be optimized for some photomultipliers.[7] However, the single electron time spread also varies with the potential distribution. A potential distribution which maximizes collection efficiency does not necessarily minimize single electron time spread. The relative collection efficiency and single electron time spread were measured as a function of the voltage ratio between the photocathode-focusing electrode and photocathode-first dynode, $(V_C-V_{FE})/(V_C-V_{D1})$, to determine optimum photomultiplier operating conditions. The results of measurements are given in Figs. 19A and 20A for 8850 and C31024, respectively. The dashed-line curves represent typical single electron time spread, FWHM, made by averaging four measurements of each type of photomultiplier evaluated. The effect of $(V_C-V_{FE})/(V_C-V_{D1})$ ratio variations on relative collection efficiency are shown by solid curves. All measurements were done with full photocathode illumination and a 1.6 mm-diameter area of photocathode illumination.

It can be seen from Fig. 19A, that in the case of full photocathode illumination of a 8850, the electron time spread has a minimum value FWHM of 0.64 nsec for $(V_C-V_{FE})/(V_C-V_{D1}) = 0.9$. Furthermore, the collection efficiency has a maximum amount for $(V_C-V_{FE})/(V_C-V_{D1}) = 1.0$. However, it is also apparent that in the case of 1.6 mm-diameter area of photocathode illumination at the center of the photocathode, the electron time spread has a minimum value FWHM of 0.4 nsec for $(V_C-V_{FE})/(V_C-V_{D1}) = 0.85$. Furthermore, the collection efficiency is 99% for optimized value of the electron time spread. Consequently, for this particular case, the electron time spread can be easily optimized, almost without a deterioration of conditions for maximum collection efficiency. Generally, optimization of photomultiplier operating conditions to minimize electron time spread reduces its variations and absolute values, even at different positions of the photocathode sensing area. However, the electron transit time of a photomultiplier increases with decreasing $(V_C-V_{FE})/(V_C-V_{D1})$ ratio. For 8850, the dependence between the transit time t_E and the $(V_C-V_{FE})/(V_C-V_{D1})$ ratio is approximately obtained from experimental data by the equation

$$t_E \approx a - b\,\frac{V_C-V_{FE}}{V_C-V_{D1}} \quad [\text{nsec}] \qquad (1)$$

where $a = 34.7$ and $b = 2.7$.

Generally, optimization of photomultiplier operating conditions to minimize electron time spread reduces its variations and absolute amounts at different positions of the photocathode sensing area, as it can be seen from Fig. 19B. Furthermore, it can be seen from Fig. 19C that the optimization of operating conditions changes the shape of curves which represent the electron transit time difference as a function of the position of the photocathode sensing area, due to the different potential distribution in the input electron optics.

Similarly, as in the previous case, with full photocathode illumination of a C31024, the electron time spread has a minimum value FWHM of 0.45 nsec for $(V_C-V_{FE})/(V_C-V_{D1}) = 0.8$. The maximum collection efficiency is obtained when $(V_C-V_{FE})/(V_C-V_{D1}) = 1.0$. In the case of 1.6 mm-diameter area of photocathode illumination at the center of the photocathode, the electron time spread is minimum when the ratio $(V_C-V_{FE})/(V_C-V_{D1}) = 0.78$. Furthermore, the collection efficiency has an almost flat maximum, for $(V_C-V_{FE})/(V_C-V_{D1})$ ratios from 0.72 to 1.0. Consequently, for this particular case, the electron time spread can be easily optimized without deterioration of the condition for maximum collection efficiency. Also, as in the previous case, the electron transit time increases with decreasing $(V_C-V_{FE})/(V_C-V_{D1})$ ratio. For a C31024 this is expressed in an approximate equation (1), where $a = 25$ and $b = 8.6$.

In general, the behavior of collection efficiency and electron time spread curves shown in Fig. 20A should be considered as typical ones for C31024 photomultipliers. However, among four photomultipliers tested, one showed significantly different dependence of collection efficiency and electron time spread upon the value of $(V_C-V_{FE})/(V_C-V_{D1})$ than the other three units, although other typical photomultiplier characteristics were inside the minimum-maximum range values specified by the manufacturer. The collection efficiency had a sharp maximum when the ratio $(V_C-V_{FE})/(V_C-V_{D1}) = 0.54$, for a full and for 1.6 mm-diameter area of photocathode illumination. Furthermore, the electron time spread had a minimum value for $(V_C-V_{FE})/(V_C-V_{D1}) = 0.9$ with full photocathode illumination. The obtained measured value of the collection efficiency at this particular point was only 51%. In the case of illumination of a 1.6 mm-diameter area, the electron time spread had a flat minimum for values of $(V_C-V_{FE})/(V_C-V_{D1})$ from 0.55 to 1. Consequently, in the case of illumination of 1.6 mm-diameter area the optimized photomultiplier operating conditions to obtain the maximum collection efficiency and minimum electron time spread was $(V_C-V_{FE})/(V_C-V_{D1}) = 0.55$. However, in the full photocathode illumination case, the photomultiplier operating conditions should be chosen with regard to the particular application. For example, if a maximum collection efficiency is important, the ratio $(V_C-V_{FE})/(V_C-V_{D1})$ should equal 0.54. In this case, the corresponding electron time spread is 0.74 nsec FWHM. Conversely, if the single electron time spread is important for a particular application, the ratio $(V_C-V_{FE})/V_C-V_{D1})$ should have the value of 0.9. The corresponding value of the relative collection efficiency for this particular operating point is only 51%. Electron transit time difference of C31024 for nonoptimized and optimized values of the $(V_C-V_{FE})/(V_C-V_{D1})$ ratio is shown in Fig. 20B.

Concerning the relative collection efficiency and the single electron time spread, it can be said from the previous considerations that optimization of photomultiplier operating conditions should be done individually for a particular photomultiplier and for a particular application, following the method given above.

Pulse Height Resolution Measurements

The pulse height resolution capabilities of the photomultiplier are significant for the detection and measurement of very low light-level scintillations in which only a few electrons are produced. Because of the statistical variations inherent in the conversion of photons to photoelectrons and the statistical nature of the secondary emission process, the photomultiplier output signal varies from one pulse to the next, even for an equal number for incident photons. Consequently, the resulting distribution in pulse height limits the photon resolution of a photomultiplier. High resolution capability permits the elimination of a large number of single-electron dark-pulses from the low-level scintillations. Possible usage is in tritium counting, certain cases of carbon counting, and Cerenkov counter applications.

Concerning the multiple-particle pulse-height resolution capabilities of the photomultiplier, the output-pulse distribution has sharply defined peaks, if the statistical distribution of the secondary emission from dynodes follows closely a Poisson distribution. However, the observed distributions for secondary electrons vary, for different types of dynodes, from an exponential distribution to a Poisson distribution. To describe the wide variety of distributions, the Polya or negative binomial distribution for dynode secondary emission statistics has been successfully applied.[8,9] The Polya distribution is defined by the expression

$$P(x) = \frac{\mu^x}{x!}\,(1+b\mu)^{-x-1/b}\prod_{i=1}^{x-1}(1+ib) \qquad (2)$$

where $P(x)$ is the probability of observing x secondary electrons, μ is the mean value of distribution, and b is a parameter controlling the shape of the distribution. In the case of $b = o$, the Polya distribution reduces to a Poisson distribution:

$$P(x)_o = \frac{\mu^x}{x!}\,e^{-\mu} \qquad (3)$$

For $b = 1$, the Polya distribution reduces to an exponential distribution as a special case:

$$P(x)_1 = \mu^x(1+\mu)^{-(x+1)} \qquad (4)$$

Consequently, a Polya distribution as a model for dynode secondary emission statistics is capable of representing a wide range of shapes of secondary electron distributions because it contains as special extreme cases both the Poisson and exponential distributions. More specifically, numerically calculated values of the single electron spectrum, using Polya distribution as a model for dynode statistics, show how the electron distribution changes continuously from a distinctively Poisson peak in the $b = o$ limit to an exponential distribution in the $b = 1$ limit.[10] As a matter of fact, for $b > 0.5$ the distribution is approaching the exponential distribution, because the peak of the distribution moves to small pulse heights and the distribution itself has a long quasi-exponential tail.

The generating function of the Polya distribution is given by the relation:

$$Q(s) = [1 + b\mu\,(1-s)]^{-1/b} \qquad (5)$$

Hence, the mean value and the variance of the distribution are

$$\bar{n} = \left.\frac{\partial Q(s)}{\partial s}\right|_{s=1} = \left.\frac{\partial[1+b\mu(1-s)]^{-1/b}}{\partial s}\right|_{s=1} = \mu \qquad (6)$$

and

$$\sigma^2 = \left.\frac{\partial^2 Q(s)}{\partial s^2}\right|_{s=1} + \left.\frac{\partial Q(s)}{\partial s}\right|_{s=1} - \left[\left.\frac{\partial Q(s)}{\partial s}\right|_{s=1}\right]^2 = b\mu^2+\mu \qquad (7)$$

The last result shows that the standard deviation σ depends upon the mean value, according to the relation $\sigma_{Py} = (b\mu^2 + \mu)^{1/2}$ for Polya distribution. For exponential distribution and Poisson distribution the dependence is given by relations: $\sigma_e = (\mu^2 + \mu)^{1/2}$ and $\sigma_{Po} = (\mu)^{1/2}$, respectively.

It follows that in the case of a Poisson distribution the standard deviation has the smallest value in comparison with standard deviation values of Polya and exponential distributions for the same amount of the mean value in all three cases. Consequently, any departure from the Poisson distribution, in the secondary emission statistics, to Polya or exponential distribution degrades the single-electron pulse-height resolution. The theoretically calculated multiple-particle pulse-height distribution for a two stage structure, with a very high gain second stage, using Polya statistics, gives twelve distinct electron peaks which are clearly resolvable.[10] However, for photomultipliers manufactured to date, our measurements show that the best electron resolution observed permitted the resolution of only 5 or 6 distinct electron peaks. Generally, the first-electron resolution does not correlate very well with the first dynode gain for an effective dynode gain value larger than 30. Apparently, other mechanisms, as for example physical nonuniformities on the dynode surface which cause each element of the surface to have a different mean value for secondary emission, and nonuniformities of the collection efficiency of the first and second dynode,[11] as well as noise contributions in photomultiplier and measuring system, may degrade the higher electron resolution capabilities of the multi-stage photomultiplier.

The pulse-height resolution measurements of the 8850 and C31024 were done by the system shown basically in the block diagram in Fig. 18. The light emitting diode was used as a light source and the

positioning disc was removed from the photomultiplier window. The operating repetition frequency of the light-pulse generator was 5 kHz and the total number of pulses taken per distribution was approximately 10^7. The output signal from the photomultiplier was applied to a linear gate to reduce the photomultiplier noise-pulse rate. The light intensity from the light-pulse generator was adjusted by varying the distance between the photomultiplier and the end of the light guide to obtain fewer or more registered counts in a given multielectron peak. The adjustment of the light intensity was done to obtain an approximately equal number of counts in the first, second, and third electron peaks. The photoelectron pulse-height spectrums obtained on a 400 channel pulse-height analyzer are shown in Figs. 21 and 22 for the 8850 and C31024, respectively. The distributions show 5 distinct electron peaks, due to the nonuniformity of the dynode surface. All photomultipliers tested were able to resolve sharply a single electron peak. The photoelectron pulse-height spectrum was practically the same when only a small part of photocathode and also when the full photocathode was illuminated.

Conclusions

Performance characteristics measurements of photomultipliers having dynodes with cesium-activated gallium phosphide secondary emitting surfaces have been presented and discussed. Generally, all measurements were done, unless otherwise indicated, using the voltage divider network suggested by RCA for a particular photomultiplier. The operating voltage was 2500 V for 8850, 8852 and C70133B photomultipliers. The operating voltage for the C31024's was 3500 V. Measurement techniques and descriptions of measuring system were given in detail.

Determination of optimum operating conditions of photomultipliers, concerning the relative collection efficiency and single electron time spread, made in several samples of each type of photomultiplier, showed that optimization should be done individually for a particular photomultiplier and for a particular application, following the previously described method. Concerning the photoelectron pulse-height resolution capabilities, the photomultipliers having dynodes with GaP(Cs) secondary emitting surfaces are the only photomultipliers presently commercially available which are able to resolve from one up to five electron peaks. Higher electron resolution capabilities, predicted by theoretical considerations of the secondary emission statistics, are possible if dynodes with better surface and collection efficiency uniformities than those presently available are produced.

Acknowledgment

The authors would like to thank Mr. Eric Young for his help in collecting data.

This work was performed as part of the program of the Physics-Chemical Biodynamics Instrumentation Research and Development Group of the Lawrence Berkeley Laboratory, Berkeley, and was supported by the U.S. Atomic Energy Commission, Contract No. W-7405-eng-48.

References

1. R. E. Simon and B. F. Williams, Secondary-Electron Emission, IEEE Trans. Nucl. Sci., NS-15, No. 3, 167-170 (1968).

2. G. A. Morton, H. M. Smith, and H. R. Krall, The Performance of High-Gain First-Dynode Photomultipliers, IEEE Trans. Nucl. Sci., NS-16, 92-95 (1969).

3. H. R. Krall, F. A. Helvy, and D. E. Persyk, Recent Developments in GaP(Cs) Dynode Photomultipliers, IEEE Trans. Nucl. Sci., NS-17, No. 3, 71-74 (1970).

4. C. C. Lo and B. Leskovar, Evaluation of the 8850 Photomultiplier with a Cesiated Gallium-Phosphide First Dynode, Engineering Note No. 1383, September 1971, Lawrence Berkeley Laboratory, Berkeley, California.

5. C. C. Lo and B. Leskovar, Evaluation of the C70133B Photomultiplier with a Cesiated Gallium-Phosphide First Dynode, Engineering Note No. 1387, October 1971, Lawrence Berkeley Laboratory, Berkeley, California.

6. C. C. Lo and B. Leskovar, Preliminary Results of Tests of the C31024 High Speed Photomultiplier with Cesiated Gallium-Phosphide Dynodes, Engineering Note No. 1384, October 1971, Lawrence Berkeley Laboratory, Berkeley, California.

7. C. R. Kerns, Photomultiplier Single-Electron Time-Spread Measurements, IEEE Trans. Nucl. Sci., NS-14, No. 1, 449-454 (1967).

8. W. Feller, in Introduction to Probability Theory and Its Applications, Vol. 1 (Wiley, New York, 1957).

9. J. R. Prescott, A Statistical Model for Photomultiplier Single-Electron Statistics, Nucl. Instr. Methods, 39, 173-179 (1966).

10. L. A. Dietz, Use of Polya Statistics in Investigations of Secondary Electron Yields from Target Surfaces, Rev. Sci. Instr., 38, No. 9, 1332-1333, (1967).

11. Private communication with T. T. Lewis, February 1972, RCA Corporation, Lancaster, Pennsylvania.

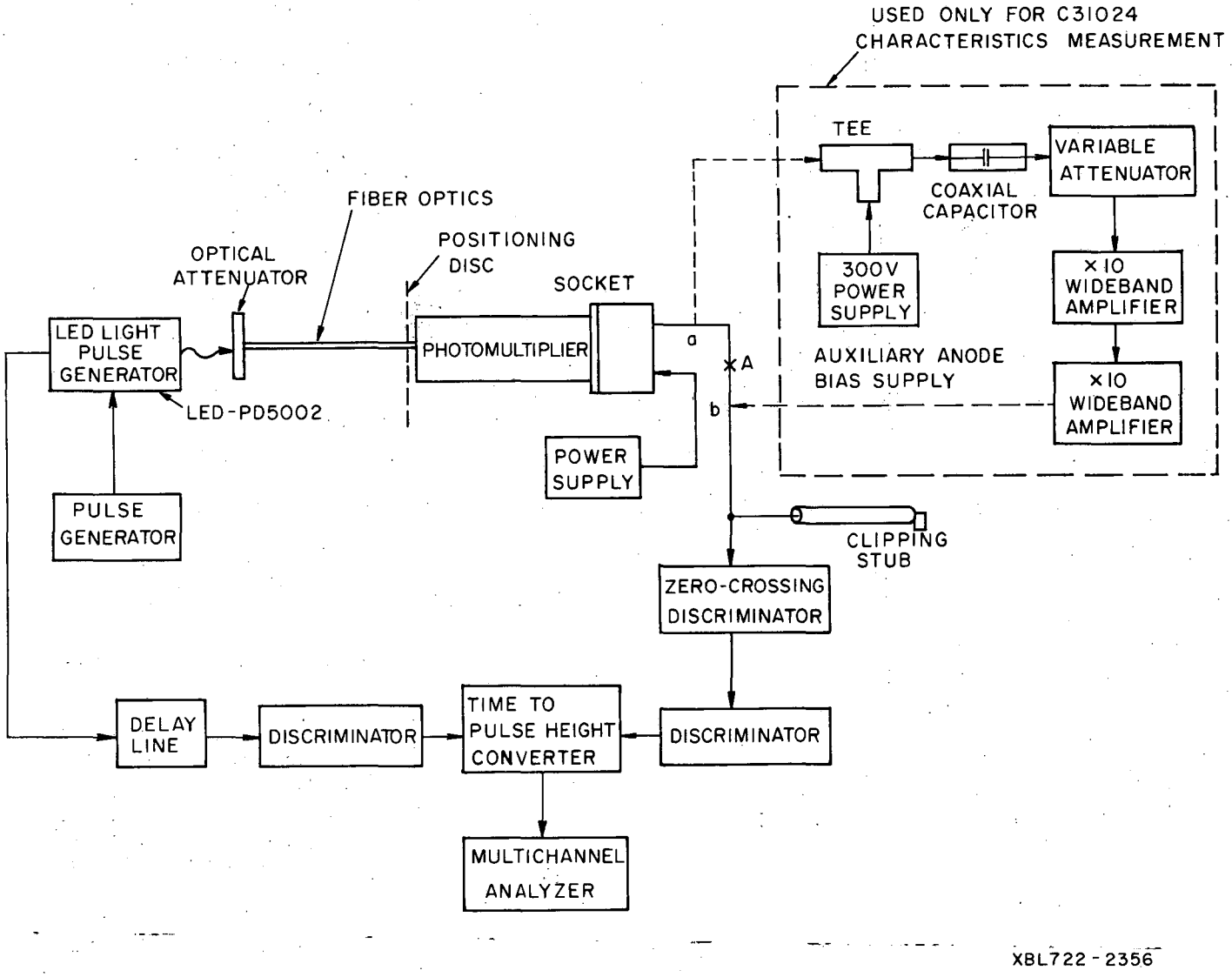

Fig. 1A - Block diagram of the system for measuring electron transit time difference and single electron time spread as a function of the position of the photocathode sensing area. The same system was used for measuring single electron time spread as a function of the voltage ratio between the photocathode-focusing electrode and photocathode-first dynode.

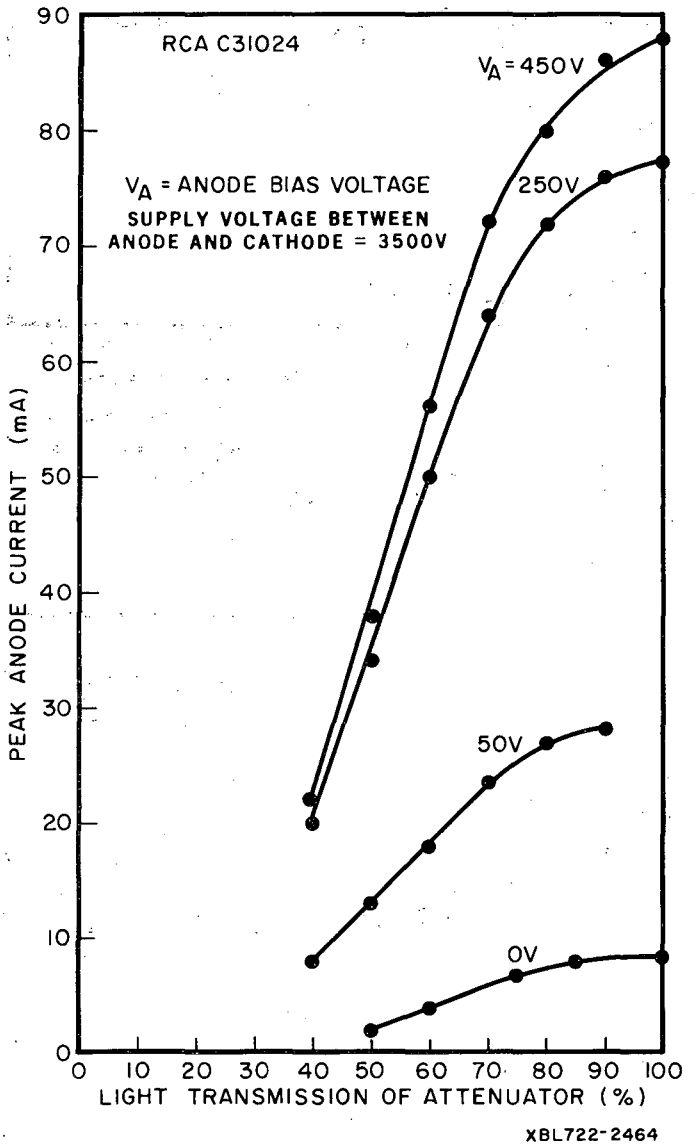

Fig. 1B - Peak anode current as a function of light transmission of the optical attenuator, with anode bias voltage as the parameter, for RCA C31024 photomultiplier.

Fig. 3 - Electron transit time difference as a function of the position of the photocathode sensing area, for RCA 8852 photomultiplier.

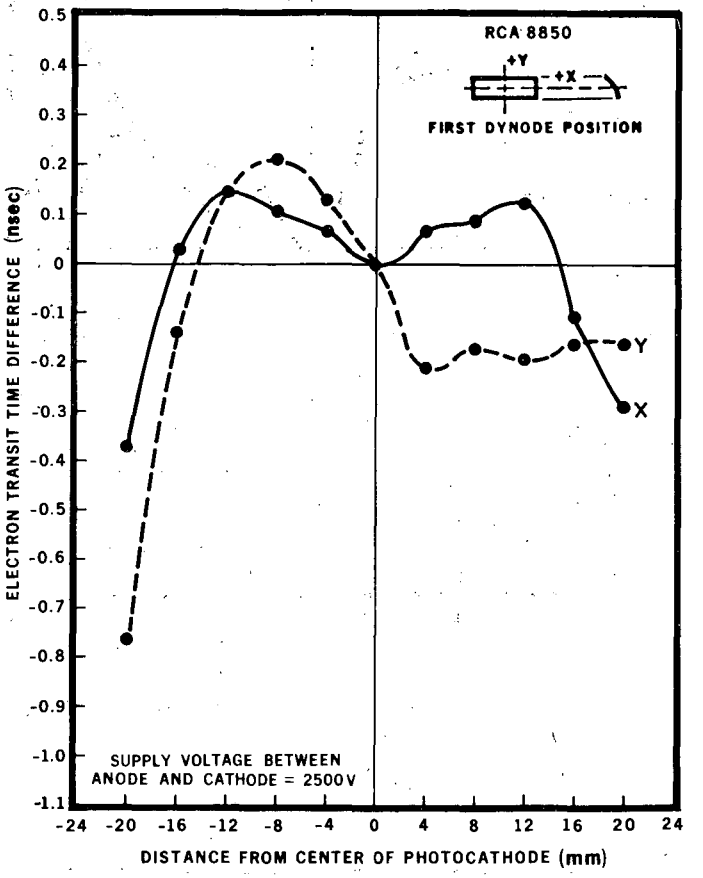

Fig. 2 - Electron transit time difference as a function of the position of the photocathode sensing area, for RCA 8850 photomultiplier.

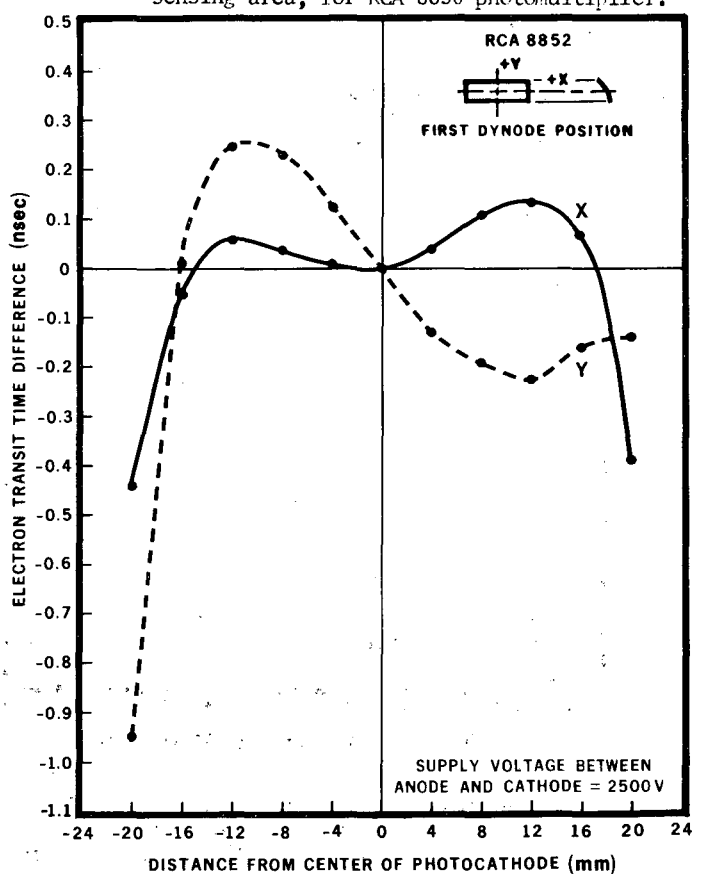

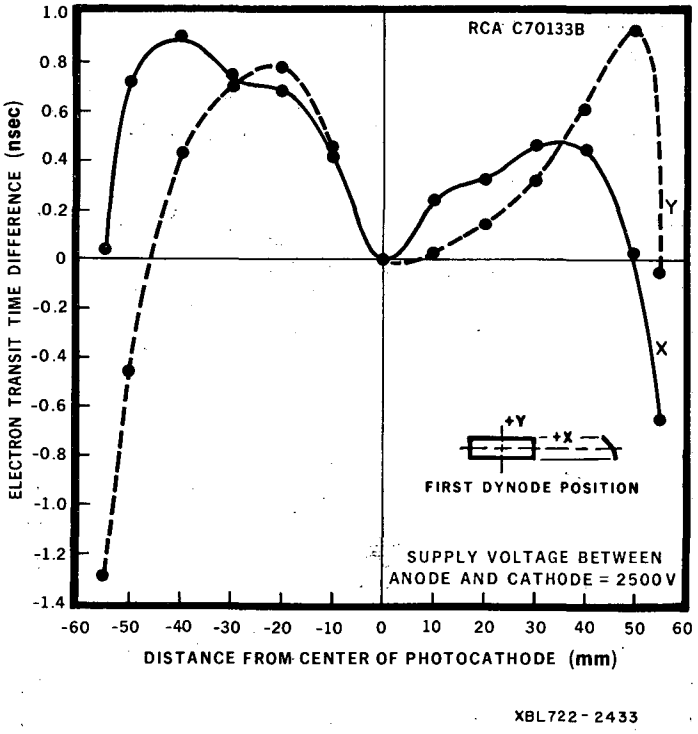

Fig. 4 - Electron transit time difference as a function of the position of the photocathode sensing area, for RCA C70133B photomultiplier.

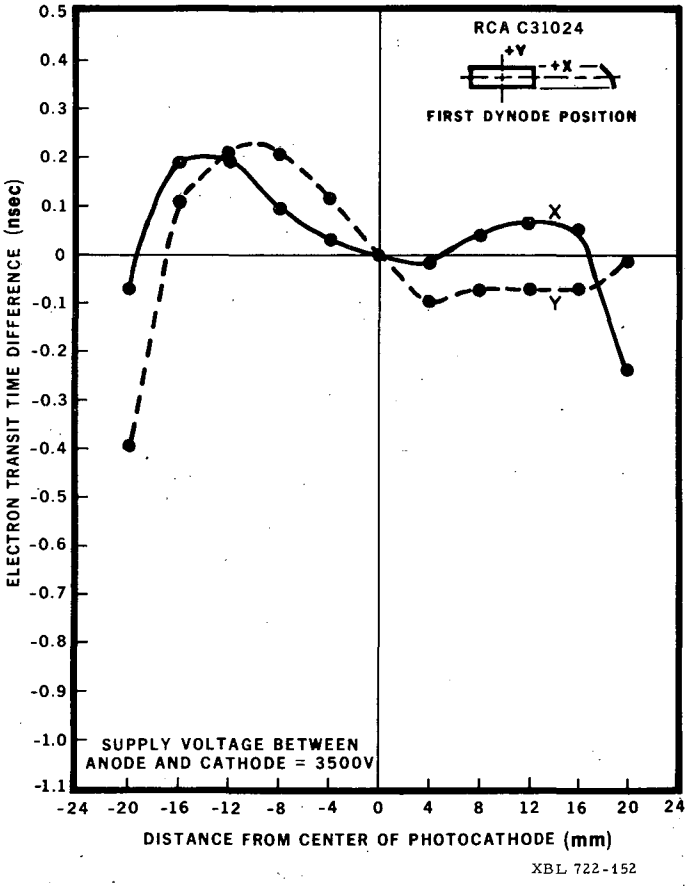

Fig. 5 - Electron transit time difference as a function of the position of the photocathode sensing area, for RCA 31024 photomultiplier.

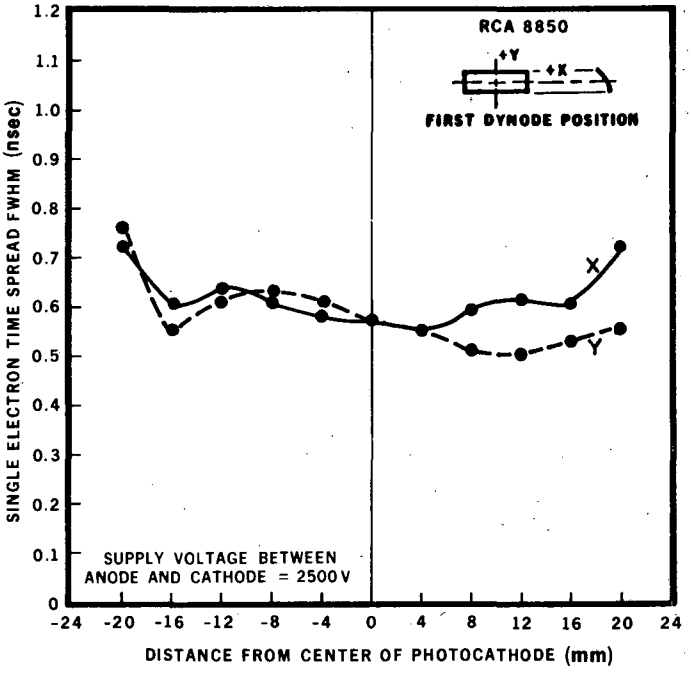

Fig. 6 - Single electron time spread as a function of the position of the photocathode sensing area, for RCA 8850 photomultiplier.

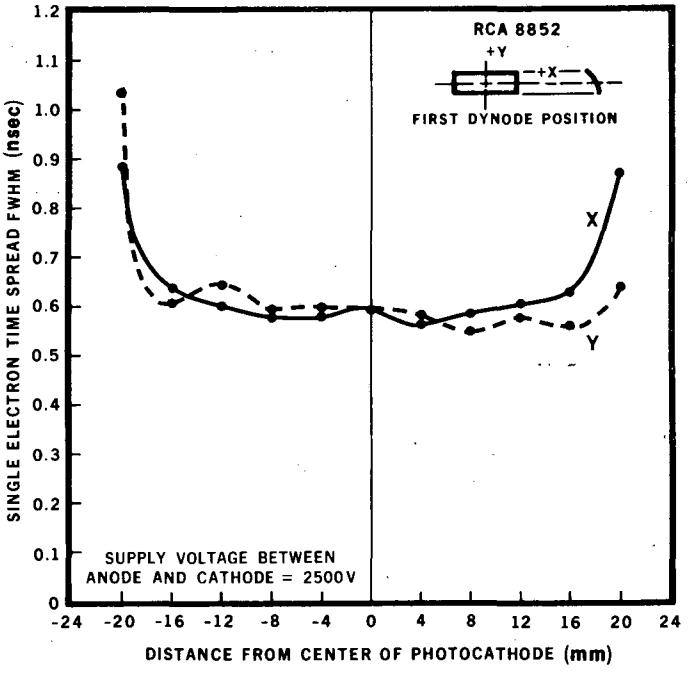

Fig. 7 Single electron time spread as a function of the position of the photocathode sensing area, for RCA 8852 photomultiplier.

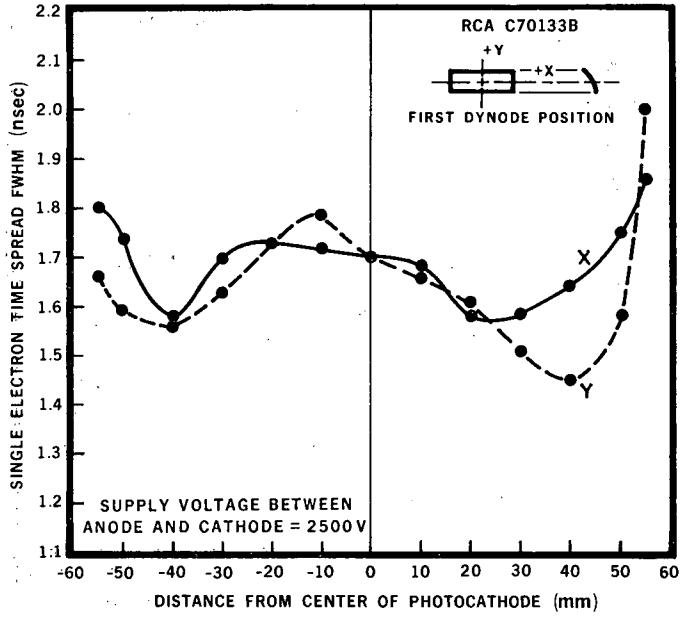

Fig. 8 - Single electron time spread as a function of the position of the photocathode sensing area, for RCA C70133B photomultiplier.

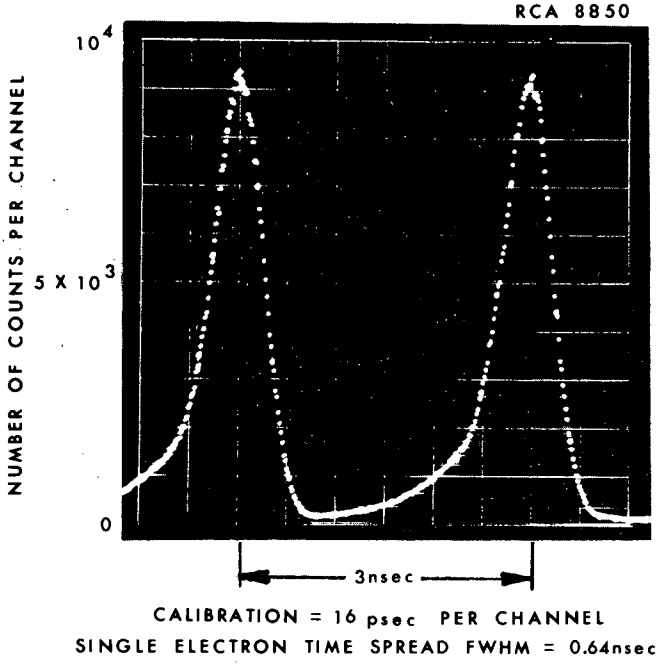

Fig. 10 - Single electron time spread of RCA 8850 photomultiplier with full photocathode illumination.

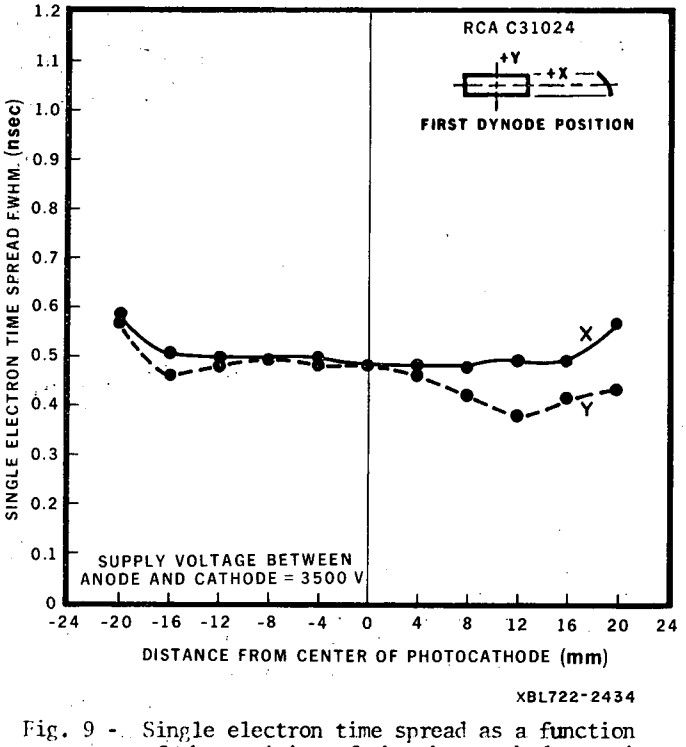

Fig. 9 - Single electron time spread as a function of the position of the photocathode sensing area, for RCA C31024 photomultiplier.

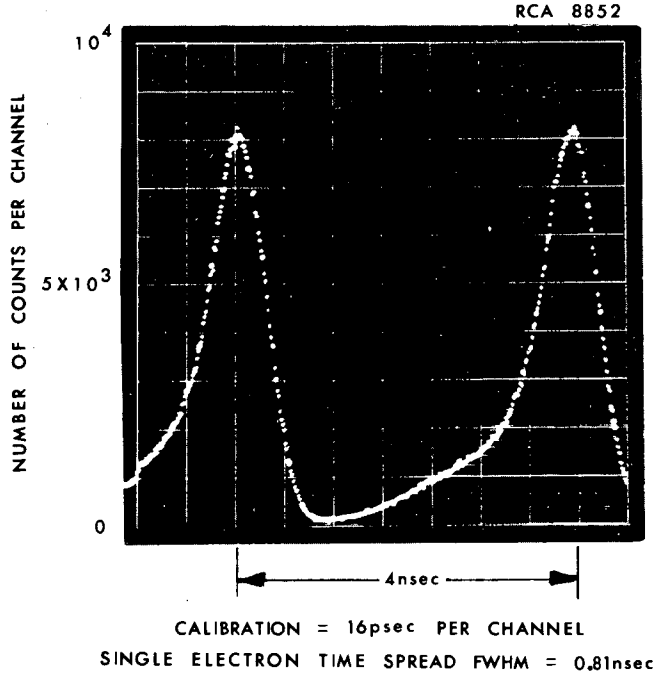

Fig. 11 - Single electron time spread of RCA 8852 photomultiplier with full photocathode illumination.

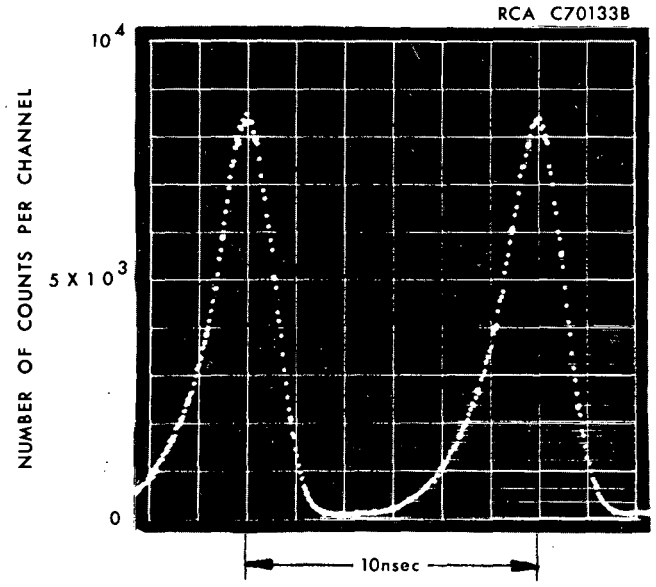

Fig. 12 - Single electron time spread of RCA C70133B photomultiplier with full photocathode illumination.

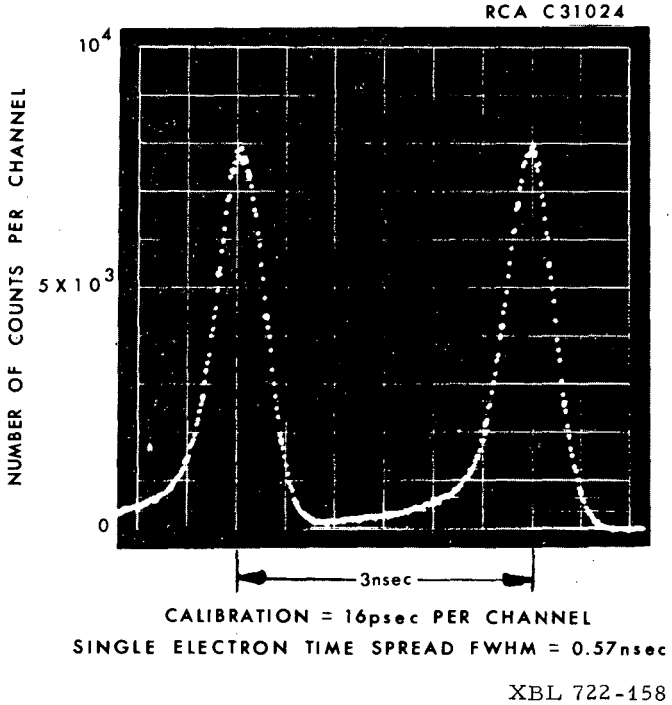

Fig. 13 - Single electron time spread of RCA C31024 photomultiplier with full photocathode illumination.

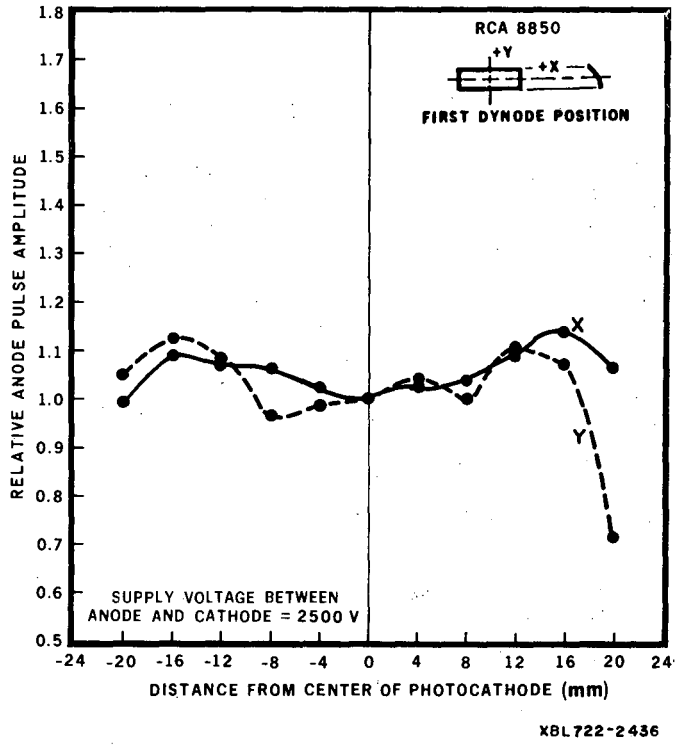

Fig. 14 - Collection and quantum efficiency uniformity as a function of the position of the photocathode sensing area, for RCA 8850 photomultiplier.

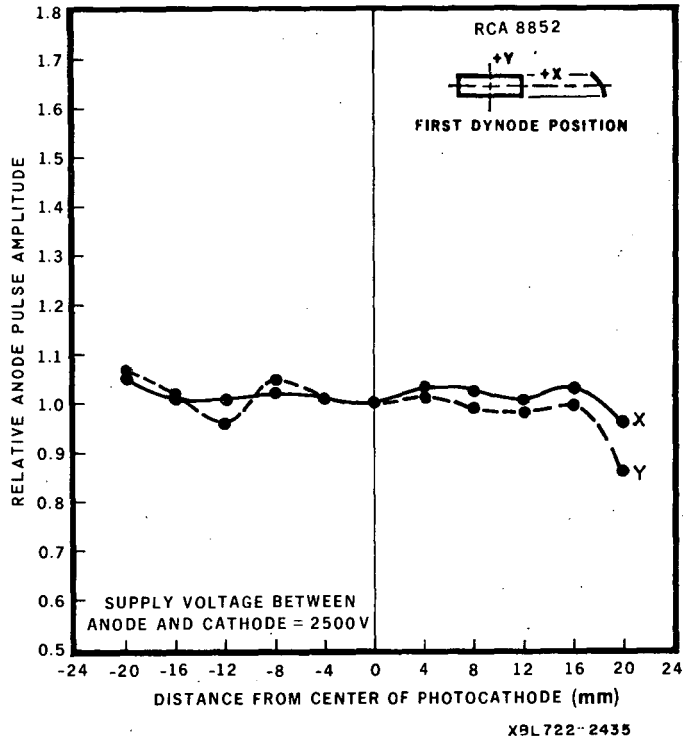

Fig. 15 - Collection and quantum efficiency uniformity as a function of the position of the photocathode sensing area, for RCA 8852 photomultiplier.

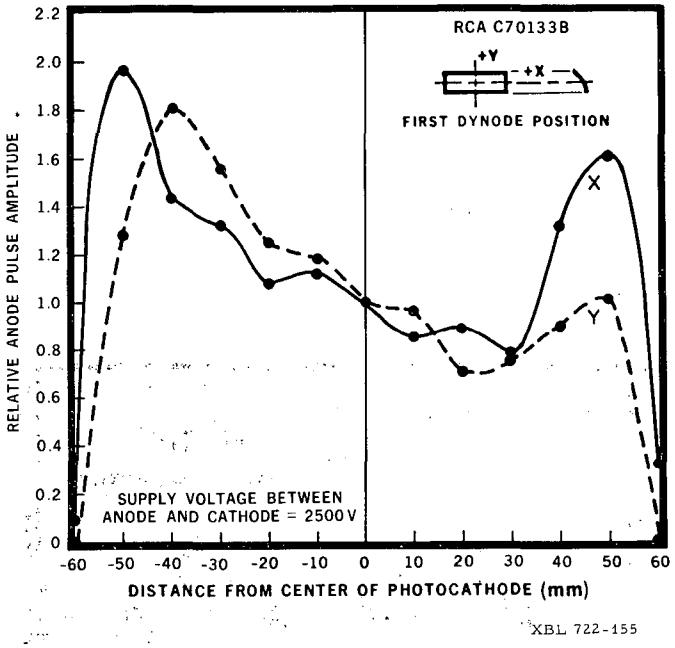

Fig. 16 - Collection and quantum efficiency uniformity as a function of the position of the photocathode sensing area, for RCA C70133B photomultiplier.

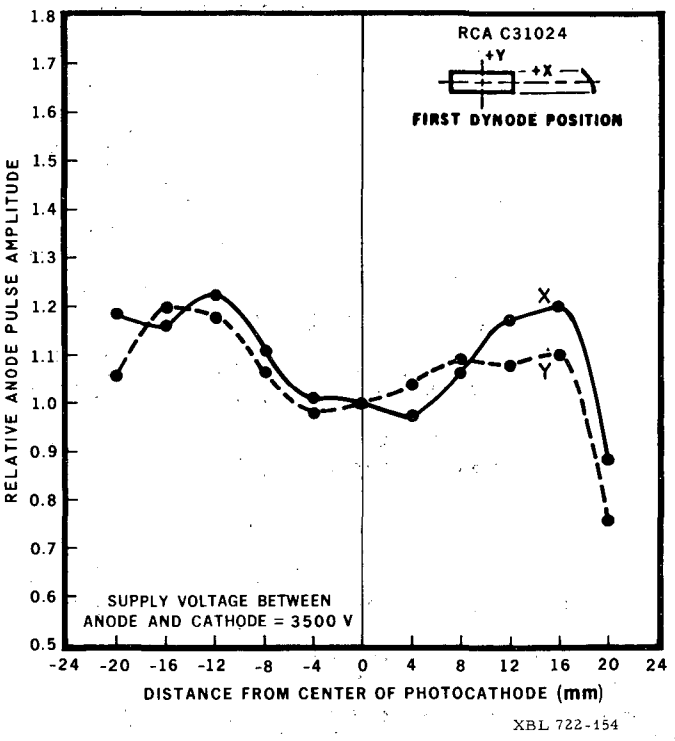

Fig. 17 - Collection and quantum efficiency uniformity as a function of the position of the photocathode sensing area, for RCA C31024 photomultiplier.

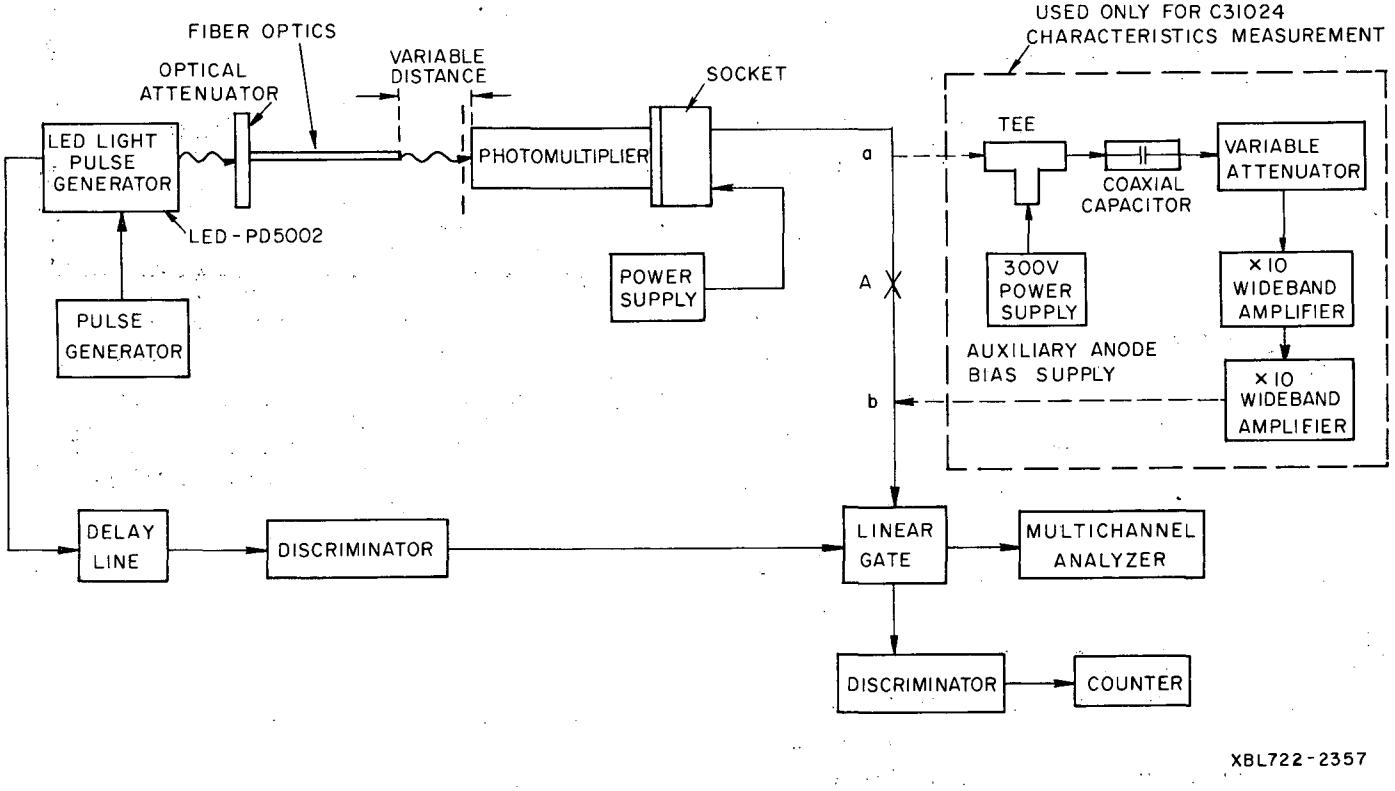

Fig. 18 - Block diagram of the system for measuring collection and quantum efficiency as a function of the position of the photocathode sensing area and photoelectron pulse-height spectrum. The same system was used for measuring relative collection efficiency as a function of the voltage ratio between the photocathode-focusing electrode and the photocathode-first dynode.

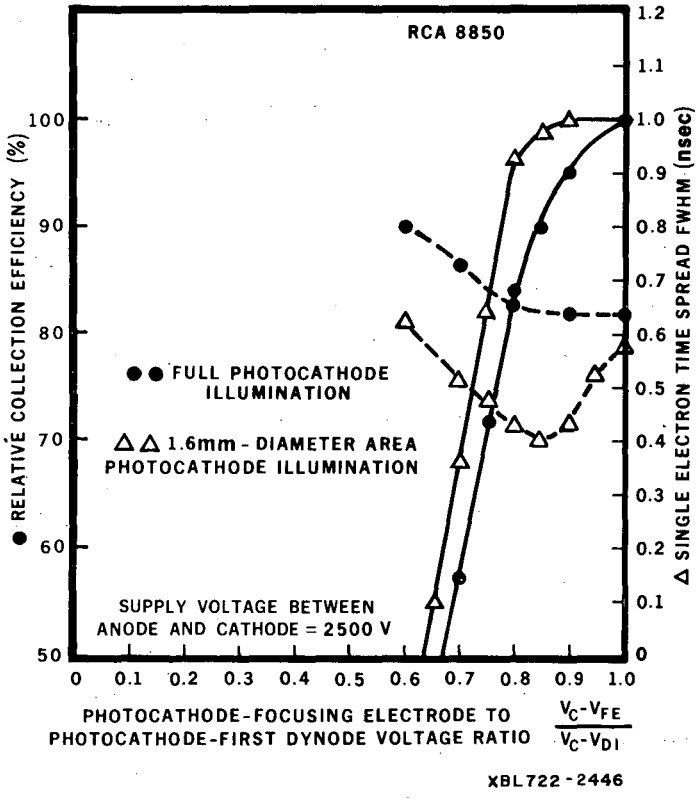

Fig. 19A - Pelative collection efficiency and single electron time spread as a function of the voltage ratio between the photocathode-focusing electrode and the photocathode-first dynode, for RCA 8850 photomultiplier.

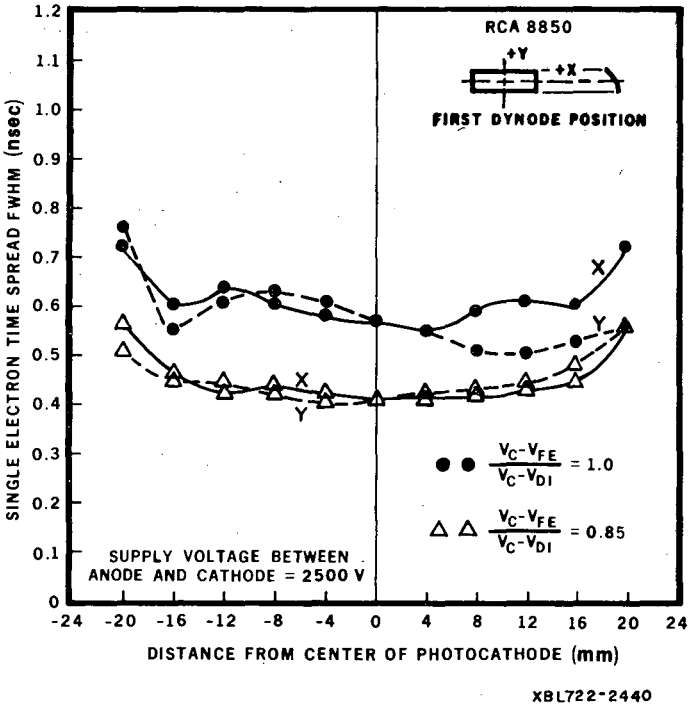

Fig. 19B - Single electron time spread of 8850 as a function of the position of the photocathode sensing area for nonoptimized and optimized values of the $(V_C-V_{FE})/(V_C-V_{D1})$ ratio.

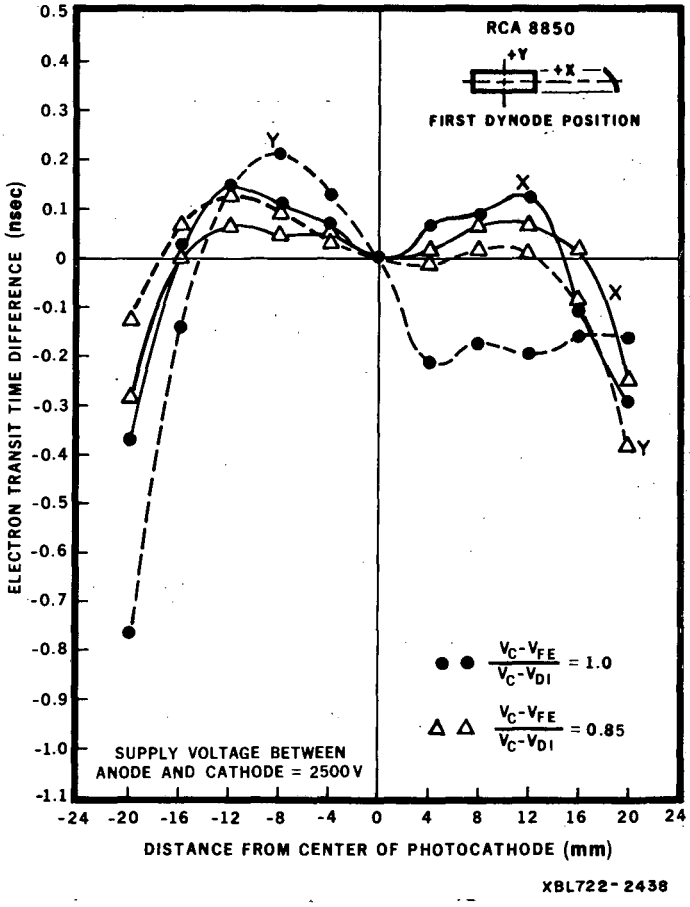

Fig. 19C - Electron transit time difference of 8850 as a function of the position of the photocathode sensing area for nonoptimized and optimized values of the $(V_C-V_{FE})/(V_C-V_{D1})$ ratio.

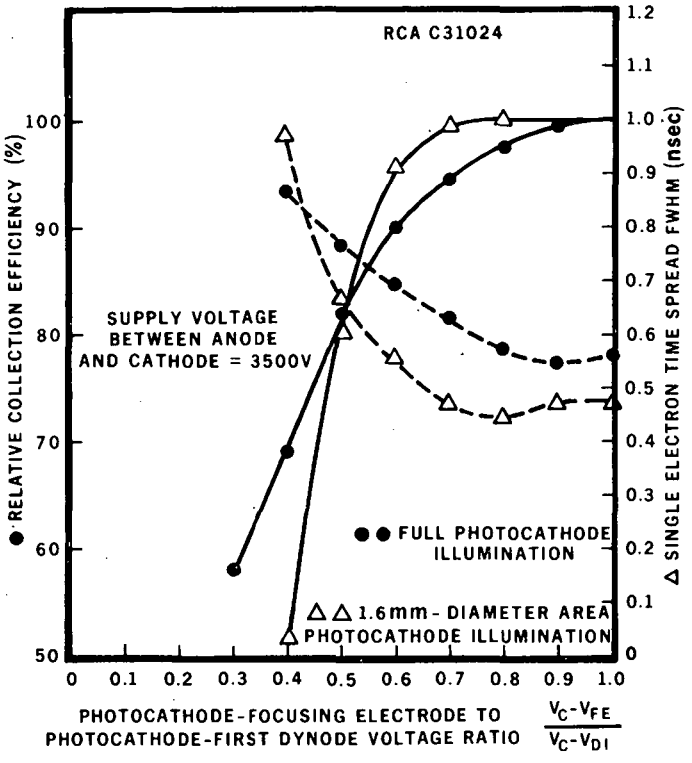

XBL722-2445

Fig.20A-Relative collection efficiency and single electron time spread as a function of the voltage ratio between the photocathode-focusing electrode and the photocathode-first dynode, for RCA C31024 photomultiplier.

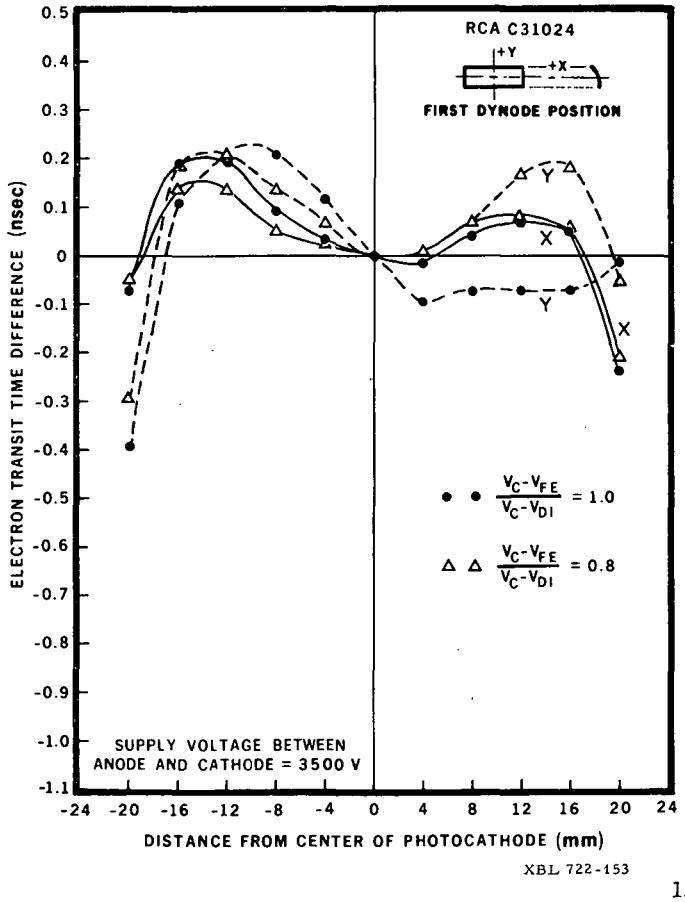

XBL 722-153

Fig. 20B - Electron transit time difference of C31024 as a function of the position of the photocathode sensing area for nonoptimized and optimized values of the $(V_C-V_{FE})/(V_C-V_{D1})$ ratio.

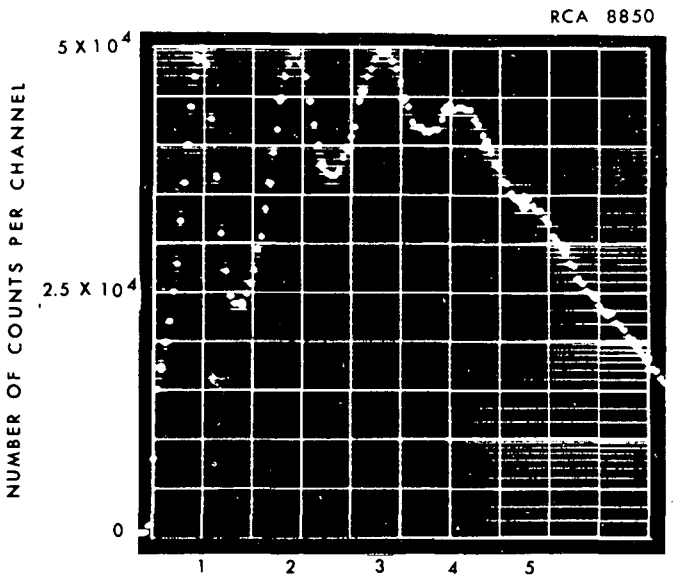

XBL 722-161

Fig. 21 - Pulse-height spectrum, showing peaks corresponding to one, two, and up to five electron peaks, for RCA 8850 photomultiplier.

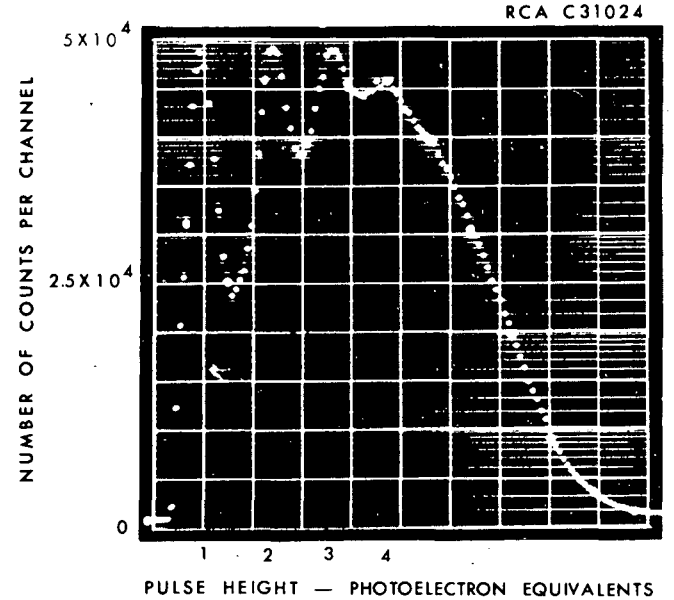

XBL 722-162

Fig. 22 - Pulse-height spectrum, showing peaks corresponding to one, two, and up to four electron peaks, for RCA C31024 photomultiplier.

TECHNICAL INFORMATION DIVISION
LAWRENCE BERKELEY LABORATORY
UNIVERSITY OF CALIFORNIA
BERKELEY, CALIFORNIA 94720